Supplement of Hydrol. Earth Syst. Sci., 28, 5353–5373, 2024
https://doi.org/10.5194/hess-28-5353-2024-supplement

Hydrology and Earth System Sciences
Open Access
EGU

Supplement of

Spatio-temporal patterns and trends of streamflow in water-scarce Mediterranean basins

Laia Estrada et al.

Correspondence to: Laia Estrada (lestrada@icra.cat)

S1 Analysis of trends in model residuals

The model residuals (observed - simulated) were analysed for temporal trends which could be attributed to the influence of increasing forest cover or density on streamflow. During the period 2000-2018 there has been an increase in forested area from 46% to 56% (EEA, 2000, 2018), but our model only considers the 2018 forested area for the whole simulation period. If the hypothesis that these land use changes are a main driver for streamflow reduction is true, the model would tend to underestimate flow at the beginning of the simulation, due to overestimating the extent of the forested area. Thus, we would expect to observe a decreasing trend in model residuals.

However, we must consider that the increase in forested area varies locally, and not all gauging stations have observed data for the whole period (2001-2022). Therefore, we have used the Corine Land Cover maps from 2000, 2006, 2012 and 2018 (EEA, 2000, 2006, 2012, 2018) to determine for each gauging station the increase in forested area within their drainage area during the closest period to the actual observations (Table S1). Of the 50 gauging stations, most (74%) present an increase in forested area, consistent with the general increase for the whole study area, while 14% present a decrease, and the remaining 12% either do not present any change in forested area or it could not be calculated because the observations start in 2018. Therefore, if the hypothesis that these land use changes are a main driver for streamflow reduction is true, we would expect to observe decreasing trends in model residuals for the gauging stations with an increase in forested area, and vice versa.

We analysed the trends of the model residuals using linear regression models. The statistical significance of trends was assessed using a student's t-test. We also used the alternative hypothesis p-values (1 – LR p-value) to classify the likelihood of each trend according to the recommendations issued by the IPCC (Mastrandrea et al., 2010): *virtually certain* ($p > 0.99$), *very likely* ($p > 0.90$), *likely* ($p > 0.66$), *about as likely as not* ($0.33 < p < 0.66$), *unlikely* ($p < 0.33$), *very unlikely* ($p < 0.10$), and *exceptionally unlikely* ($p < 0.01$).

The metrics of the trends in the model residuals are summarised in Table S1, and Fig. S1 shows the spatial distribution of trend slopes. Figure S2 shows the plots of the residuals over time. Of the 50 gauging stations analysed, 70% have a significant trend (p-value < 0.05). According to Mastrandrea et al. (2010), the likelihoods are: 62% *virtually certain*, 18% *very likely*, 6% *likely*, 10% *about as likely as not*, 2% *unlikely*, and 2% *very unlikely*. However, of the 37 gauging stations with an increase in forested area, only 54% show a decreasing trend in model residuals (55.6% when only considering statistically significant trends). Similarly, of the 7 gauging stations with a decrease in forested area, 4 show an increasing trend in model residuals, but only 2 are significant. In summary, of the 44 gauging stations where a change in forested area is observed, only 17 (38.6%) present a trend in model residuals consistent with the change. Moreover, we also must consider that R^2 is very small for all trends, with a maximum of 0.098, although 82% of trends present values of $R^2 < 0.01$. Therefore, as we do not observe clear trends in model residuals, we can reasonably assume that land use changes in our study are not a main driver influencing streamflow and their omission for the purpose of our analysis is not incorrect.

Table S1. Trends in the model residuals and change in forested area in the catchment area of each gauging station. Significant trends are marked in bold (p-value < 0.05). LR: Linear Regression. The units for LR slopes are $m^3/s/day$.

Gauging station	Change in forested area (%)	LR slope	LR p-value	R^2	Likelihood
Abrera	+16.13	-7.43E-04	**5.55E-04**	3.21E-03	virtually certain
Balsareny	+11.60	2.74E-04	**3.49E-18**	9.55E-03	virtually certain
Berga	+0.71	2.25E-04	**4.21E-07**	4.91E-03	virtually certain
Cardona	-1.27	2.00E-04	**1.14E-17**	1.08E-02	virtually certain
Castellar de n'Hug	+10.26	1.60E-05	**2.71E-02**	7.93E-04	very likely
Castellbell i el Vilar	+16.05	5.04E-04	**3.69E-16**	8.31E-03	virtually certain
Castellbisbal	-1.59	2.25E-04	1.93E-01	5.58E-04	likely
Castellet i la Gornal	+16.89	-1.26E-05	**3.39E-03**	2.08E-03	virtually certain
El Papiol	+7.26	3.68E-05	**4.20E-03**	2.10E-03	virtually certain
Esponellà	+8.09	-3.20E-04	**5.70E-12**	6.00E-03	virtually certain
Fogars de la Selva (Can Simó)	+4.99	-2.07E-04	**1.64E-15**	8.84E-03	virtually certain
Fogars de la Selva (Pont Eiffel)	+2.05	-1.05E-04	**2.22E-05**	2.42E-03	virtually certain
Girona (Onyar)	+19.66	-1.65E-06	9.35E-01	8.18E-07	very unlikely
Girona (Ter)	+8.64	-1.10E-04	3.96E-01	9.36E-05	about as likely as not
Guardiola de Berguedà	+14.72	1.42E-04	**1.96E-07**	3.47E-03	virtually certain
Guixers (Aigua de Valls)	0	8.39E-04	**7.85E-23**	2.19E-02	virtually certain
Guixers (Cardener - Monegal)	-	-7.24E-04	**1.38E-34**	9.80E-02	virtually certain
Jorba	+20.84	-1.08E-05	6.43E-02	9.39E-04	very likely
La Cellera de Ter	+8.71	2.24E-04	1.35E-01	3.39E-04	likely
La Coma i la Pedra	+32.51	-2.33E-04	**2.05E-11**	1.73E-02	virtually certain
La Garriga	+9.62	3.55E-05	**6.73E-09**	4.19E-03	virtually certain
La Pobla de Claramunt	-0.37	-2.85E-05	**4.83E-09**	8.48E-03	virtually certain
Les Masies de Roda (Ter i Gurri)	+8.05	3.38E-04	**1.42E-05**	2.95E-03	virtually certain
Les Masies de Roda (Ter)	-0.13	-4.37E-04	**4.90E-02**	1.26E-03	very likely
Martorell	-0.26	-9.67E-06	8.40E-01	9.89E-06	unlikely
Montornès del Vallès	+6.65	-1.25E-05	**9.17E-03**	9.57E-04	virtually certain
Montseny	+20.40	-3.41E-06	6.52E-01	3.57E-05	about as likely as not
Navès	+10.24	1.98E-05	7.38E-02	6.49E-04	very likely
Olot	+6.48	-7.09E-05	**1.27E-14**	7.67E-03	virtually certain
Puig-reig	-3.58	2.04E-05	1.76E-01	4.04E-04	likely
Ripoll	+7.43	9.11E-05	6.15E-02	4.35E-04	very likely
Riudellots de la Selva	+11.10	-1.91E-04	**2.43E-34**	2.40E-02	virtually certain
Sallent	+14.88	3.81E-05	**4.14E-11**	6.75E-03	virtually certain
Sant Celoni	+12.71	-2.90E-06	6.22E-01	3.08E-05	about as likely as not
Sant Feliu de Buixalleu	+9.10	4.65E-05	**7.89E-03**	1.91E-03	virtually certain
Sant Gregori	+5.72	-4.30E-05	**3.03E-05**	3.13E-03	virtually certain
Sant Joan de les Abadesses	+9.36	5.34E-05	**2.58E-02**	6.28E-04	very likely

Sant Joan Despí	+14.78	5.75E-04	**9.37E-08**	3.73E-03	virtually certain
Sant Sadurní d'Anoia	+14.53	2.43E-05	9.73E-02	3.54E-04	very likely
Sant Vicenç dels Horts	-1.48	1.56E-03	**7.14E-20**	1.38E-02	virtually certain
Santa Coloma de Gramenet	+5.48	-1.17E-04	**5.37E-06**	2.84E-03	virtually certain
Santa Cristina d'Aro	+36.08	3.14E-06	8.01E-02	5.22E-04	very likely
Santa Perpètua de Mogoda	+2.90	-1.04E-04	**1.10E-24**	2.79E-02	virtually certain
Serra de Daró	+11.39	-8.87E-05	**7.51E-03**	1.09E-03	virtually certain
Torelló	0	1.21E-04	**2.92E-02**	1.62E-03	very likely
Torroella de Montgrí	+9.54	-4.62E-04	**9.68E-03**	8.90E-04	virtually certain
Tortellà	+0.69	-3.08E-04	**1.94E-06**	1.05E-02	virtually certain
Vilada (Merdançol)	0	-3.75E-06	4.59E-01	2.02E-04	about as likely as not
Vilada (Riera Vilada)	0	2.36E-05	4.87E-01	1.41E-04	about as likely as not
Vilanova de Sau	-	1.00E-03	**9.33E-13**	5.01E-02	virtually certain

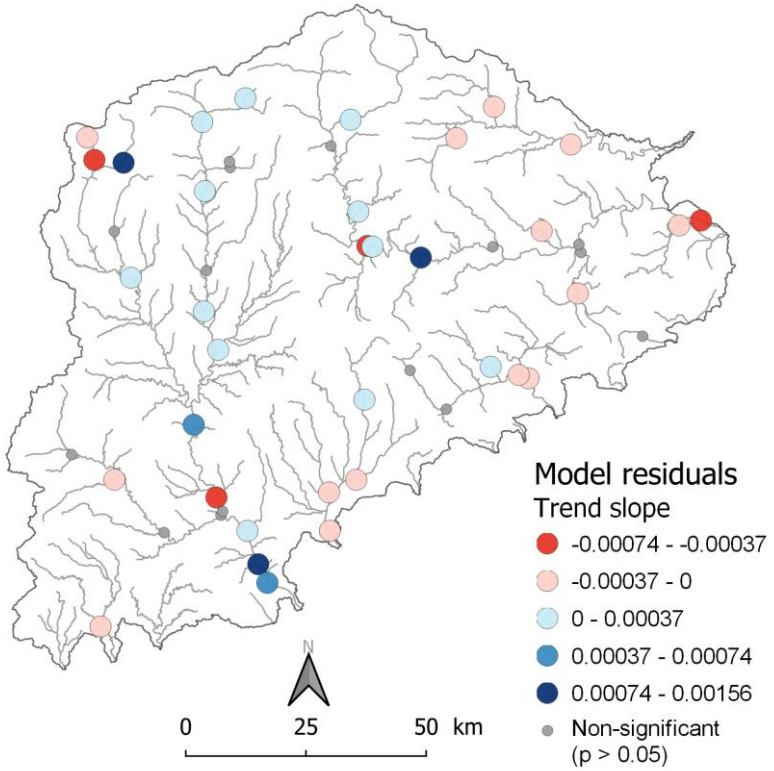

Figure S1: Spatial distribution of trend slopes (units $m^3/s/day$) for model residuals.

Figure S2: Plots of model residuals over time for each of the 50 gauging stations.

S2 Uncertainty of simulated streamflow

We quantified the uncertainty associated with the simulated streamflow with 95PPU bands (Abbaspour et al., 2015, 2018). These bands are calculated at the 2.5% and 97.5% levels of the cumulative distribution of simulated streamflow obtained through Latin hypercube sampling, and their goodness of fit is assessed by the metrics "P-factor" and "R-factor". The P-factor, varying from 0 to 1, is the fraction of observed data bracketed by the 95PPU band, and the R-factor is the ratio of the average width of the 95PPU band and the standard deviation of the observed data. For assessing discharge, it is recommended that the P-factor and R-factor are respectively > 0.7 and < 1.5, although smaller P-factors might be considered acceptable depending on the scale of the project (Abbaspour et al., 2015).

Table S2 lists the R-factor and P-factor for each SWAT+ model. The R-factor for all models is below the recommended value, but most P-factors do not reach the recommended 0.7. Nevertheless, Abbaspour et al. (2015) reports gauging stations with P-factor as low as 0.39 as accurate, and taking into account satisfactory R-factor and KGE values, we consider this uncertainty acceptable.

Table S2. R-factor and P-factor of the 95PPU bands.

SWAT+ model	P-factor	R-factor
Llobregat	0.48	0.47
Ter	0.50	0.45
Besòs-Tordera	0.75	0.36
Fluvià	0.65	0.31
Foix	0.65	0.41

For each of the six gauging stations in Fig. 2, Fig.s S3-S8 show the observed daily streamflow, the (best) simulated daily streamflow, and the 95PPU bands for each gauging station respectively.

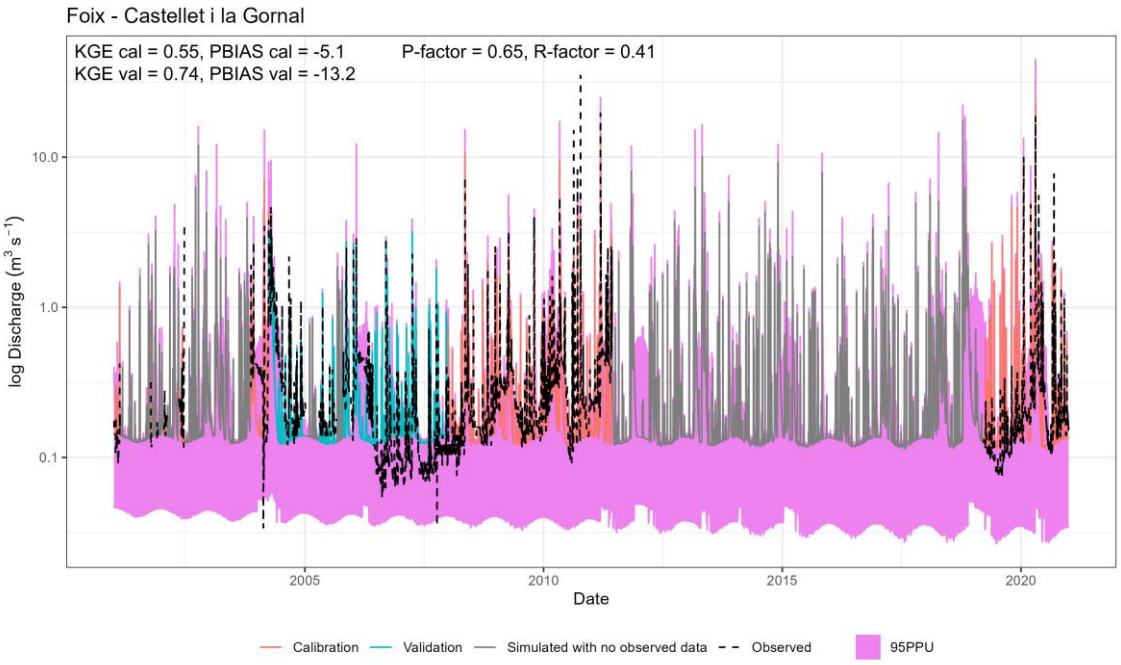

Figure S3: Observed and simulated daily streamflow, and the 95PPU band for the gauging station in Castellet i la Gornal, in the Foix basin. KGE and PBIAS values for the calibration and validation periods and the R-factor and P-factor are shown.

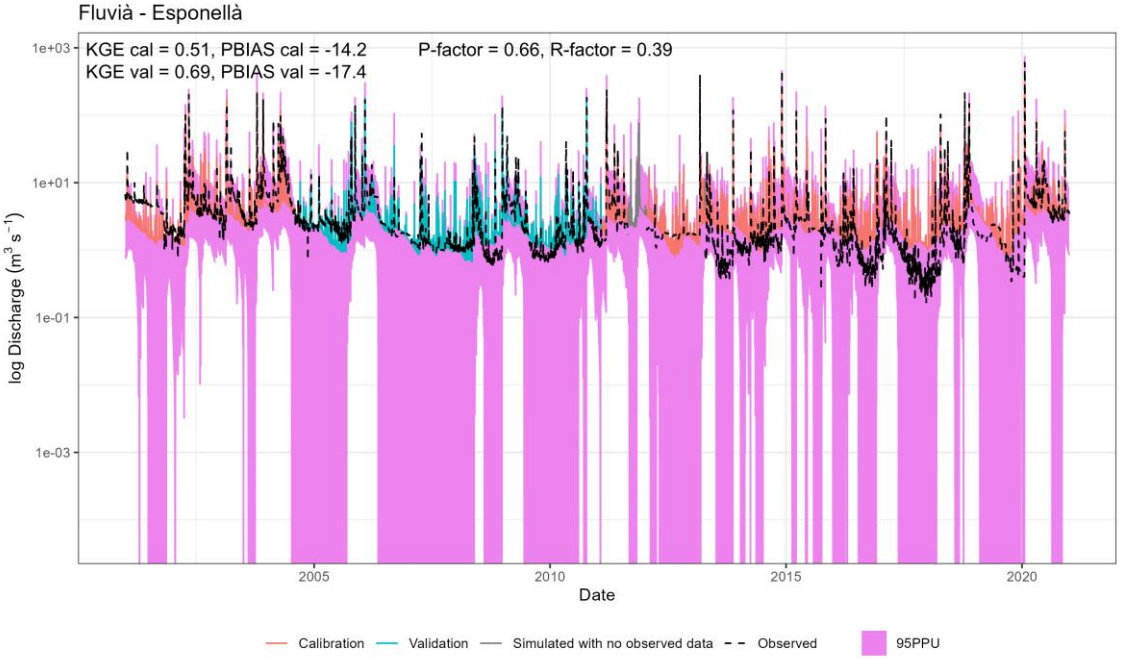

Figure S4: Observed and simulated daily streamflow, and the 95PPU band for the gauging station in Esponellà, in the Fluvià basin. KGE and PBIAS values for the calibration and validation periods and the R-factor and P-factor are shown.

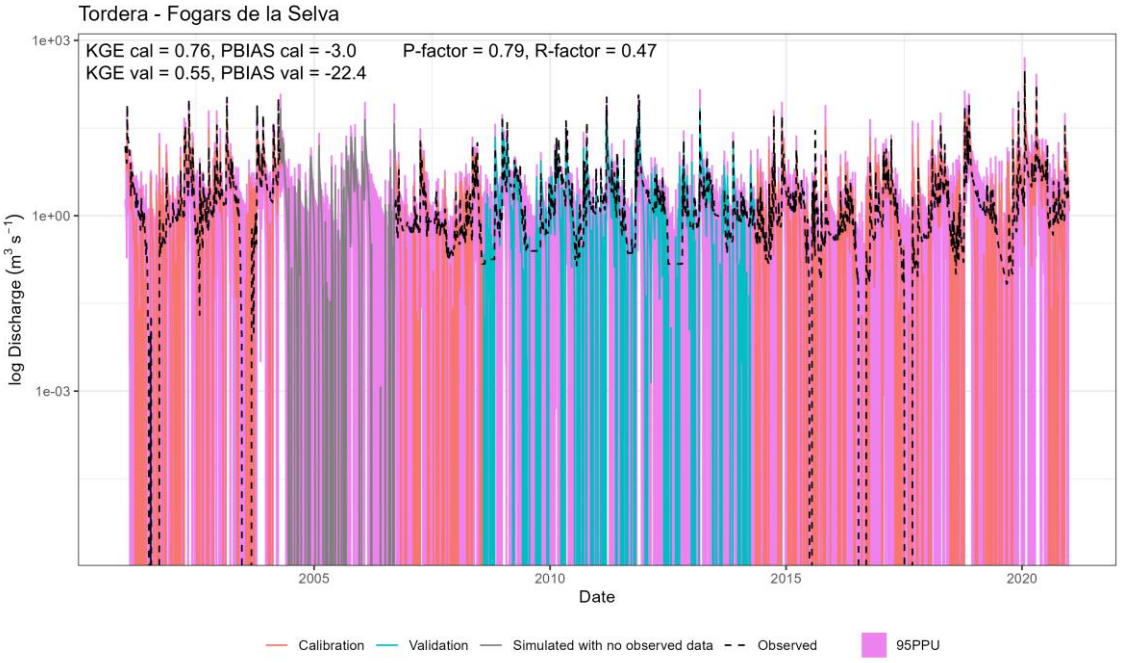

Figure S5: Observed and simulated daily streamflow, and the 95PPU band for the gauging station in Fogars de la Selva, in the Tordera basin. KGE and PBIAS values for the calibration and validation periods and the R-factor and P-factor are shown.

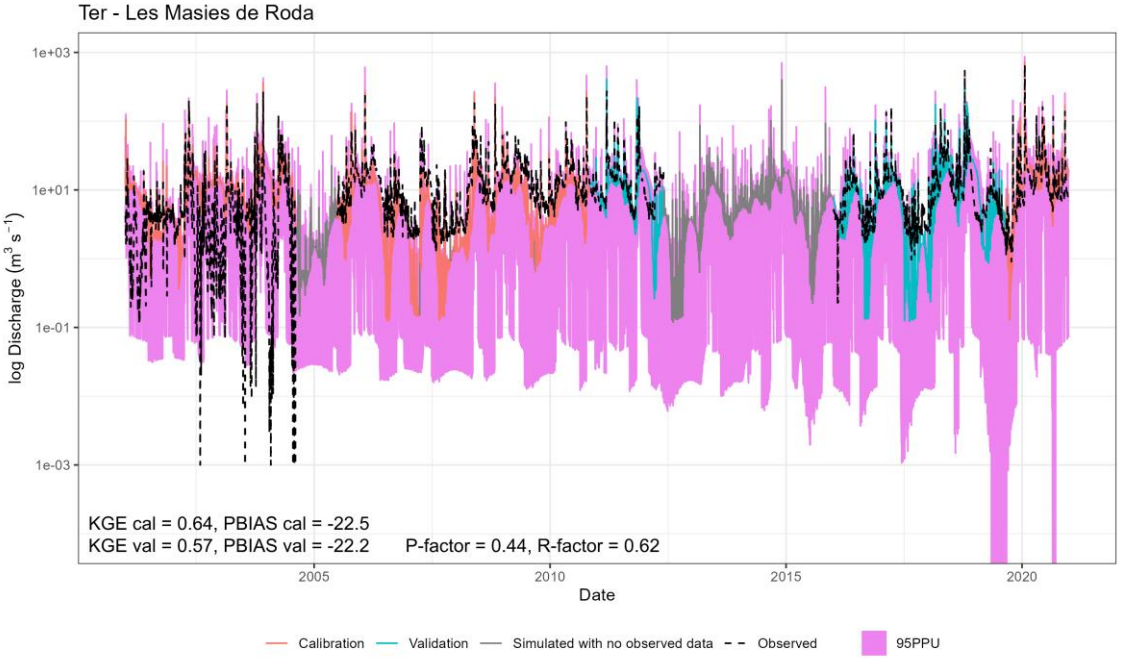

Figure S6: Observed and simulated daily streamflow, and the 95PPU band for the gauging station in Les Masies de Roda, in the Ter basin. KGE and PBIAS values for the calibration and validation periods and the R-factor and P-factor are shown.

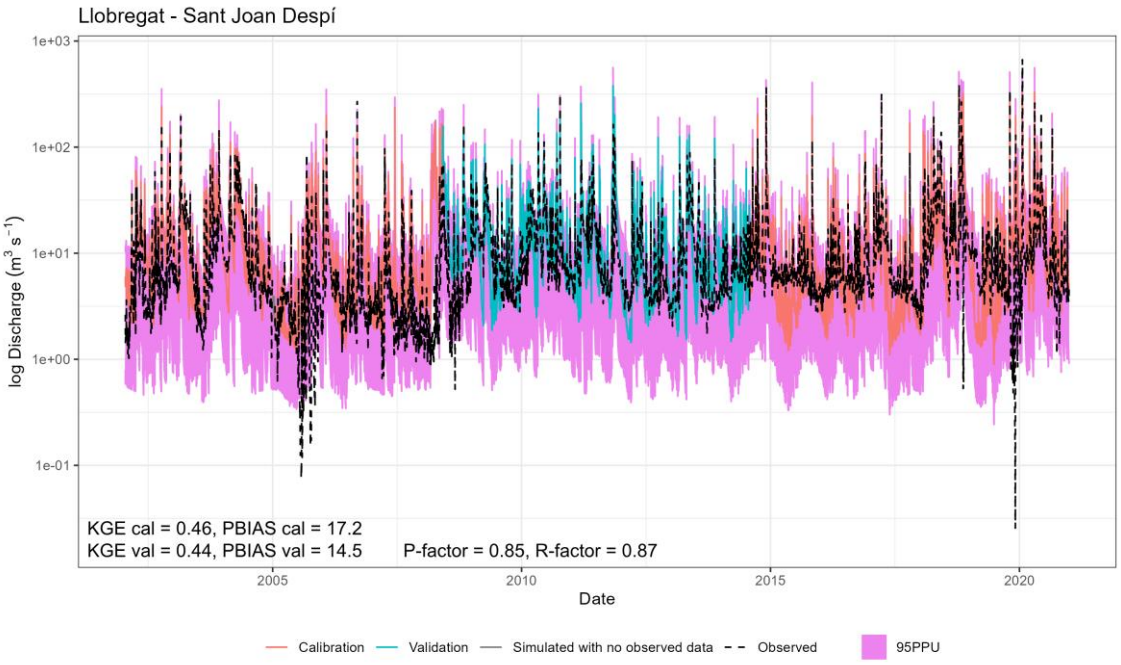

Figure S7: Observed and simulated daily streamflow, and the 95PPU band for the gauging station in Sant Joan Despí, in the Llobregat basin. KGE and PBIAS values for the calibration and validation periods and the R-factor and P-factor are shown.

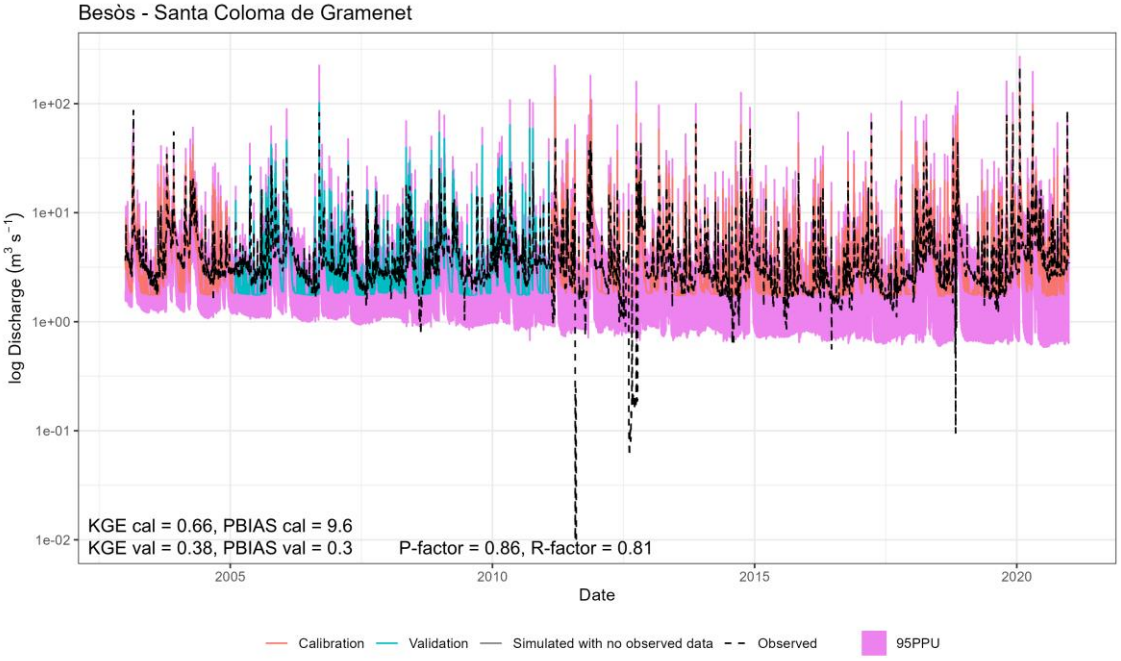

Figure S8: Observed and simulated daily streamflow, and the 95PPU band for the gauging station in Santa Coloma de Gramenet, in the Besòs basin. KGE and PBIAS values for the calibration and validation periods and the R-factor and P-factor are shown.

S3 Comparison of observed and simulated trends

Using simulated streamflow to calculate hydrological indicators and then identifying their trends provides us with comprehensive results in both time and space, as opposed to only using observed data, which allows us to only identify trends at specific locations and gaps in the record hinder the analysis.

Nevertheless, we compared the observed and the simulated trends at four of the gauging stations with the most complete record of all CRBD. Missing data, especially when it consists of several contiguous days, may compromise the calculation of some indicators, and thus the analysis of trends. However, we are able to calculate all indicators for the four gauging stations by omitting missing data.

Figure S9 shows the observed and simulated Sen's slopes of each of the 40 indicators, while Fig. S10 shows only the indicators for which both the observed and simulated trend are significant (Mann-Kendall, p-value < 0.05), as well as the uncertainty associated to the simulated Sen's slopes due to model equifinality. While some of the significant pairs present different directions, the majority are both either positive or negative, even considering the uncertainty. Therefore, while we might not capture all the significant trends present in the observations, we can confirm that using simulated streamflow to fill spatial and temporal gaps in the observed record allows us to better identify and characterize spatio-temporal trends.

Table S3. Hydrological indicators and their labels used in Figs. S9 and S10.

Figure label	Hydrological indicator	Figure label	Hydrological indicator
1	Median of daily flow in January	21	7-day means of maximum daily flow
2	Median of daily flow in February	22	30-day means of minimum daily flow
3	Median of daily flow in March	23	30-day means of maximum daily flow
4	Median of daily flow in April	24	90-day means of minimum daily flow
5	Median of daily flow in May	25	90-day means of maximum daily flow
6	Median of daily flow in June	26	Julian date of minimum daily flow
7	Median of daily flow in July	27	Julian date of maximum daily flow
8	Median of daily flow in August	28	Number of high pulses
9	Median of daily flow in September	29	Number of low pulses
10	Median of daily flow in October	30	Mean duration of high pulses
11	Median of daily flow in November	31	Mean duration of low pulses
12	Median of daily flow in December	32	Rise rate
13	Median of annual daily flow	33	Fall rate
14	10th percentile of annual daily flow	34	Number of flow reversals
15	90th percentile of annual daily flow	35	Total number of days with zero-flow
16	Annual minimum daily flow	36	Frequency of zero-flow events
17	Annual maximum daily flow	37	Mean duration of zero-flow events
18	3-day means of minimum daily flow	38	jday of first zero-flow event
19	3-day means of maximum daily flow	39	Median jday of zero-flow events
20	7-day means of minimum daily flow	40	Sum of all annual flow

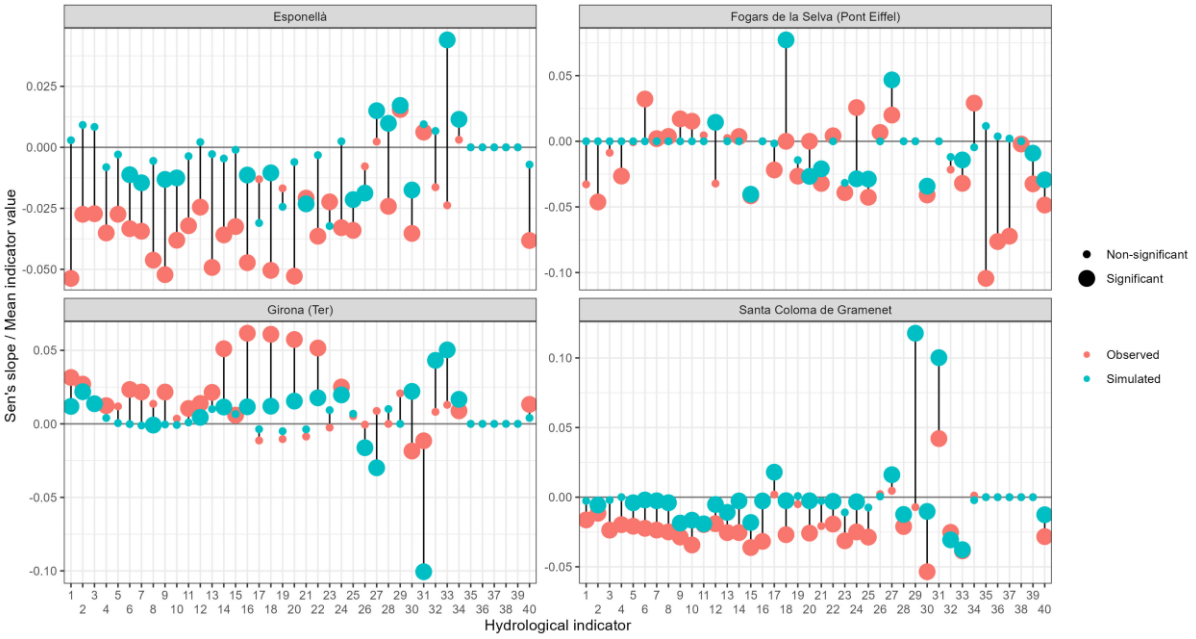

Figure S9: Ratio of Sen's slope to mean indicator value for observed and simulated trends. See Table S3 to match each indicator to the number used in the figure.

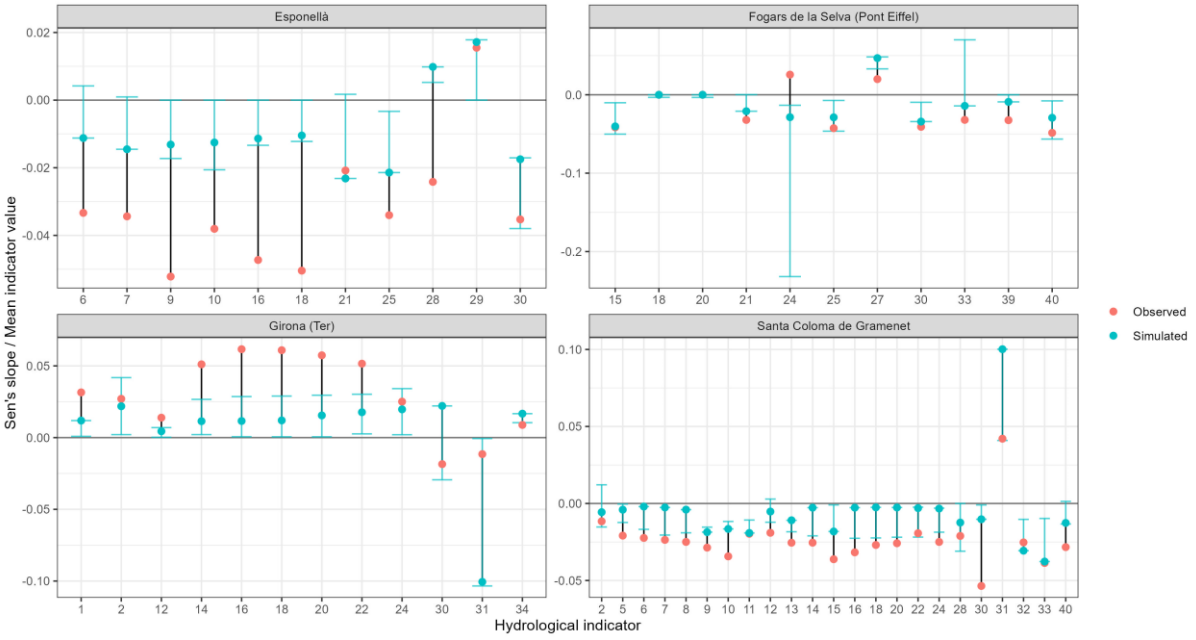

Figure S10: Ratio of Sen's slope to mean indicator value only for significant pairs of observed and simulated trends. Uncertainty associated to simulated Sen's slope is also shown. For indicators 18 and 20 in the Fogars de la Selva plot, the Sen's slope is not divided by the indicator value. This is because due to the Sen's slope being very close to 0, the uncertainty value became too large when standardizing, and so it masked the other indicators. See Table S3 to match each indicator to the number used in the figure.

References

Abbaspour, K., Rouholahnejad, E., Vaghefi, S., Srinivasan, R., Yang, H., and Kløve, B.: A continental-scale hydrology and water quality model for Europe: Calibration and uncertainty of a high-resolution large-scale SWAT model, J. Hydrol., 524, 733–752, https://doi.org/10.1016/J.JHYDROL.2015.03.027, 2015.

Abbaspour, K., Vaghefi, S. A., and Srinivasan, R.: A Guideline for Successful Calibration and Uncertainty Analysis for Soil and Water Assessment: A Review of Papers from the 2016 International SWAT Conference, Water, 10, 6, https://doi.org/10.3390/W10010006, 2018.

European Environment Agency (EEA): Corine Land Cover (CLC) 2000, Version 2020_20u1, https://land.copernicus.eu/en/products/corine-land-cover/clc-2000, 2000.

European Environment Agency (EEA): Corine Land Cover (CLC) 2006, Version 2020_20u1, https://land.copernicus.eu/en/products/corine-land-cover/clc-2006, 2006.

European Environment Agency (EEA): Corine Land Cover (CLC) 2012, Version 2020_20u1, https://land.copernicus.eu/en/products/corine-land-cover/clc-2012, 2012.

European Environment Agency (EEA): Corine Land Cover (CLC) 2018, Version 2020_20u1, https://land.copernicus.eu/en/products/corine-land-cover/clc2018, 2018.

Mastrandrea, M. D., Field, C. B., Stocker, T. F., Edenhofer, O., Ebi, K. L., Frame, D. J., Held, H., Kriegler, E., Mach, K. J., Matschoss, P. R., Plattner, G.-K., Yohe, G. W., and Zwiers, F. W.: Guidance Note for Lead Authors of the IPCC Fifth Assessment Report on Consistent Treatment of Uncertainties, 2010.